

## Article

# Synthesis of Si/C Composites by Silicon Waste Recycling and Carbon Coating for High-Capacity Lithium-Ion Storage

Jinning Huang <sup>1,†</sup>, Jun Li <sup>2,†</sup>, Lanxin Ye <sup>1</sup>, Min Wu <sup>1</sup>, Hongxia Liu <sup>3</sup>, Yingxue Cui <sup>2</sup> , Jiabiao Lian <sup>2</sup>  
and Chuan Wang <sup>1,\*</sup>

<sup>1</sup> Institute of Advanced Synthesis, School of Chemistry and Molecular Engineering, Jiangsu National Synergetic Innovation Center for Advanced Materials, Nanjing Tech University, Nanjing 211816, China; hjn18856617552@163.com (J.H.); yeah\_0509@163.com (L.Y.); 202061105024@njtech.edu.cn (M.W.)

<sup>2</sup> Institute for Energy Research, Jiangsu University, Zhenjiang 212013, China; li42485115@163.com (J.L.); yxcui@ujs.edu.cn (Y.C.); jblian@ujs.edu.cn (J.L.)

<sup>3</sup> College of Electrical Engineering and Control Science, Nanjing Tech University, Nanjing 211816, China; lhx\_ccc@126.com

\* Correspondence: ias\_cwang@njtech.edu.cn

† These authors contributed equally to this work.

**Abstract:** It is of great significance to recycle the silicon (Si) kerf slurry waste from the photovoltaic (PV) industry. Si holds great promise as the anode material for Li-ion batteries (LIBs) due to its high theoretical capacity. However, the large volume expansion of Si during the electrochemical processes always leads to electrode collapse and a rapid decline in electrochemical performance. Herein, an effective carbon coating strategy is utilized to construct a precise Si@C<sub>PPy</sub> composite using cutting-waste silicon and polypyrrole (PPy). By optimizing the mass ratio of Si and carbon, the Si@C<sub>PPy</sub> composite can exhibit a high specific capacity and superior rate capability (1436 mAh g<sup>-1</sup> at 0.1 A g<sup>-1</sup> and 607 mAh g<sup>-1</sup> at 1.0 A g<sup>-1</sup>). Moreover, the Si@C<sub>PPy</sub> composite also shows better cycling stability than the pristine prescreen silicon (PS-Si), as the carbon coating can effectively alleviate the volume expansion of Si during the lithiation/delithiation process. This work showcases a high-value utilization of PV silicon scraps, which helps to reduce resource waste and develop green energy storage.

**Keywords:** waste recycling; silicon scraps; carbon coating; Si/C composites; anode materials



**Citation:** Huang, J.; Li, J.; Ye, L.; Wu, M.; Liu, H.; Cui, Y.; Lian, J.; Wang, C. Synthesis of Si/C Composites by Silicon Waste Recycling and Carbon Coating for High-Capacity Lithium-Ion Storage. *Nanomaterials* **2023**, *13*, 2142. <https://doi.org/10.3390/nano13142142>

Academic Editor: Carlos Miguel Costa

Received: 8 June 2023

Revised: 8 July 2023

Accepted: 13 July 2023

Published: 24 July 2023



**Copyright:** © 2023 by the authors. Licensee MDPI, Basel, Switzerland. This article is an open access article distributed under the terms and conditions of the Creative Commons Attribution (CC BY) license (<https://creativecommons.org/licenses/by/4.0/>).

## 1. Introduction

With the development of the global economy, non-renewable resources such as oil and natural gas can no longer meet people's needs. Therefore, the development of a series of renewable resources has gradually become a research hotspot, and among them, solar energy has attracted much attention [1]. In recent years, the photovoltaic industry, as the core of solar cells, has mainly developed silicon-based solar cells, meaning that the large-scale photovoltaic (PV) industry inevitably produced abundant silicon (Si) kerf slurry waste, causing the waste of resources and environmental pollution issues [2,3]. Therefore, it is important to find a method that can not only recover the silicon powder in the waste residue of the PV industry, but also to discover anode materials for lithium-ion batteries with excellent electrochemical performance.

LIBs are widely used as energy storage devices in daily life, and their advantages are having a high energy density and a long cycle life. With the increasing energy density of LIBs, the supply of traditional carbon-based materials has fallen short in the energy market. Therefore, the development of rationally designed new anode materials has become a core research topic [4–8]. Much research has focused on the development of high-capacity active materials and components to improve the energy density and performance of next-generation LIBs. Among them, silicon has a high theoretical specific capacity, which is

ten times that of graphite. Silicon-based materials, which are more prominent among non-carbon-based materials, have become the most promising candidates for the new generation of lithium-ion battery anodes due to their high specific capacity [9,10], abundant natural reserves, and environmental friendliness [11]. Conversely, despite the advantages mentioned above, in the process of lithiation/delithiation, the volume of silicon will reach 120–400% [4], resulting in the crushing of silicon particles, the splitting and dispersion of electrode materials, and the damage of electrode structure, thus affecting the long-term cycle stability of lithium-ion batteries. Meanwhile, the volume effect will cause the rupture of silicon and the continuous formation of new solid electrolyte interphase (SEI) layers [12], resulting in a decline of Coulombic efficiency (CE), an increase in battery internal resistance, poor rate performance, poor conductivity, and battery failure, thus limiting the commercial application of silicon anodes. Therefore, it is still a huge challenge to design silicon composites [13].

For the practical application of power batteries to meet the requirements of higher energy density and fast charging of batteries, it is required that the design of Si/C materials should fully consider the specific capacity per unit volume and the structural stability of the material under high current impact [14,15]. At the same time, attention should be paid to improving the cycle life and poor conductivity of silicon anode materials. Although it is an effective way to slow down the volume expansion by adjusting the pore structure, it will also lead to low tap density and thus low battery volume capacity [16]. Therefore, carbon coating becomes an effective method to alleviate the stress caused by volume expansion and increase the conductivity of silicon materials [17–26]. In addition, the first step towards commercialization is to reduce costs so that they can be used in production. Consequently, it is essential to seek simple, inexpensive, and pollution-free silicon raw materials and to develop simple and effective preparation processes.

Crystalline silicon cutting waste silicon raw-Si from Shangrao Jinko Photovoltaic Power Generation Co, Ltd, Jiangxi Province, China (particle size is 1–100  $\mu\text{m}$ ) was ball-milled, pickled, and calcined to remove the organic compounds in the waste silicon powder, and the structure remained unchanged, small particle flakes of prescreen silicon (PS-Si) with micron/irregular superimposition were presented. The long-cycle performance and stability of raw-Si and PS-Si as LIBs anode materials at 0.1 A  $\text{g}^{-1}$  for 300 cycles were investigated. The charge–discharge specific capacities of the waste silicon before treatment were 356  $\text{mAh g}^{-1}$  and 1073  $\text{mAh g}^{-1}$ , respectively. After pretreatments such as pickling and ball milling, the charge–discharge specific capacities were 1397  $\text{mAh g}^{-1}$  and 3106  $\text{mAh g}^{-1}$ , respectively, and the ICE was also increased from 33% to 44%. The content of impurities such as metal elements and organics was high in the waste silicon before being treated, which reduced the capacity of silicon (theoretical capacity is 4200  $\text{mAh g}^{-1}$ ), and after 20 cycles, the specific capacity of both dropped to about 50  $\text{mAh g}^{-1}$ . However, after pretreatment, the first charge–discharge specific capacity and ICE were improved. The main reason for the low capacity is due to the significant volume expansion in the process of silicon lithiation; during the continuous cycle of lithiation/delithiation in LIBs, silicon repeatedly expands and contracts, and the electrodes are pulverized, which eventually leads to the attenuation of the lithium storage capacity. This work not only increases the value of waste silicon and reduces the resource waste, but also promotes the development of high-capacity anode materials for green energy storage.

## 2. Experimental

### 2.1. Synthesis of Silicon Hydroxylation

As shown in Figure S1, 15 mL of  $\text{H}_2\text{O}_2$  was slowly added to 45 mL of concentrated  $\text{H}_2\text{SO}_4$ , and then placed in an oil bath and heated to 80  $^\circ\text{C}$ . Afterward, prescreen silicon (PS-Si) suspension was hydroxylated on its silicon surface, then washed with water and dried to obtain PS-Si-OH with hydroxyl groups attached to the surface.

## 2.2. Synthesis of Mesoporous Silicon/Carbon Composites

An appropriate amount of PS-Si-OH powder was dissolved in deionized water, and then 200  $\mu\text{L}$ , 400  $\mu\text{L}$ , and 800  $\mu\text{L}$  of polypyrrole (PPy) were added into the above solution, respectively. After cooling for 30 min, 100 mg, 200 mg, and 400 mg of ammonium persulfate were poured into the above solution, respectively. After stirring in the ice bath for 12 h, the products were obtained and named Si@PPy-1, Si@PPy-2, Si@PPy-3, respectively. The Si@PPy were centrifugally washed with water and alcohol, and then dried. Finally, Si@PPy were heated to 400  $^{\circ}\text{C}$  for 1 h under an  $\text{N}_2$  atmosphere. The Si@C<sub>PPy</sub>-1, Si@C<sub>PPy</sub>-2, and Si@C<sub>PPy</sub>-3 composites were obtained.

Detailed descriptions about characterization methods and electrochemical measurements are given in the supplementary material.

## 3. Results and Discussion

The morphology of Si@C<sub>PPy</sub> composites were examined by scanning electron microscopy (SEM). As shown in Figure S2a–c, Si@C<sub>PPy</sub>-1, Si@C<sub>PPy</sub>-2, and Si@C<sub>PPy</sub>-3 present nanosheet-like structures. Compared with the SEM image of PS-Si (Figure S3), the carbon material is coated on the surface of silicon nanosheets and maintains a sheet-like structure. To better understand the structure of Si@C<sub>PPy</sub>-2 composites, high-resolution TEM and energy dispersive X-ray spectroscopy (EDX) tests were carried out. As shown in Figure 1b, the Si nanoflakes are coated with an amorphous carbon layer from the carbonization of Ppy, which reduces the volume expansion of Si. In addition, as shown in the EDX element mapping (Figure 1c–f), the uniform distribution of Si and C is consistent with the uniform carbon layer coated on the surface of Si nanosheets.

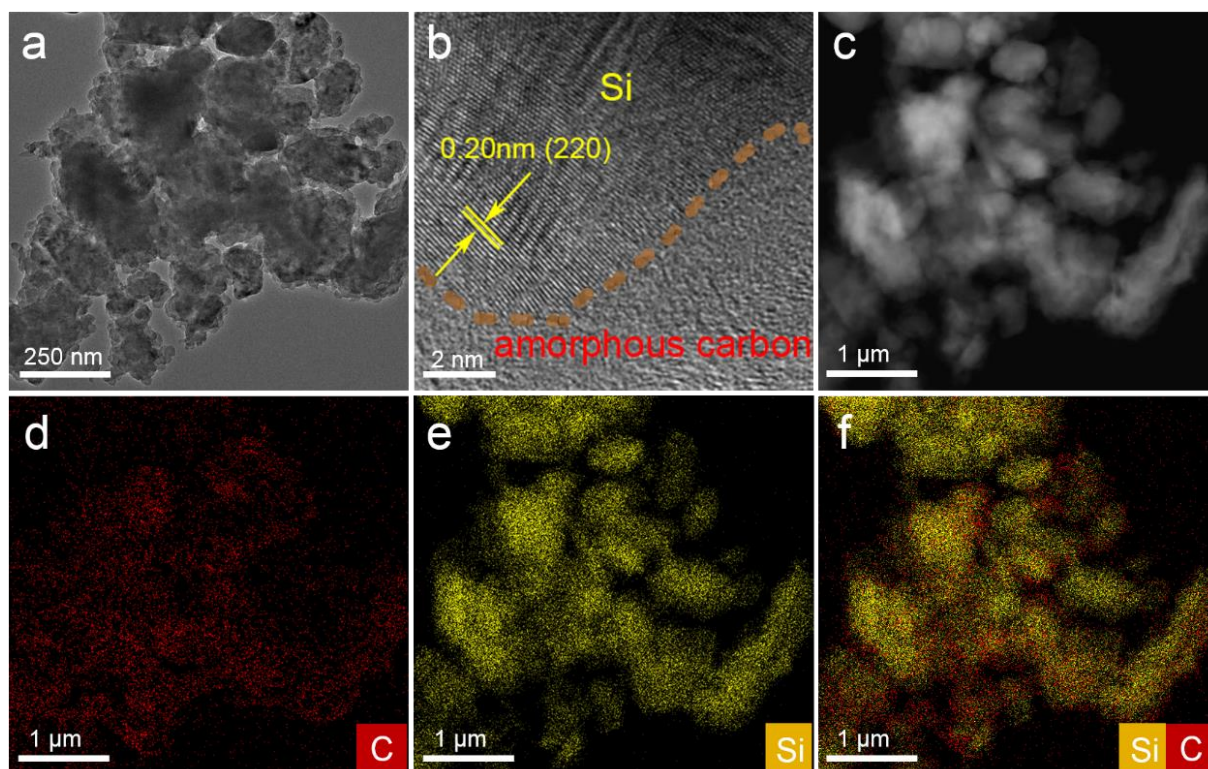


**Figure 1.** (a) TEM, (b) HRTEM, (c) HAADF, and (d–f) elemental mapping images of Si@C<sub>PPy</sub>-2.

To prove that the carbon was successfully coated on the silicon surface, XRD and Raman tests were performed. Figure 2a and Figure S4a show five peaks at  $2\theta = 28^{\circ}$ ,  $47^{\circ}$ ,  $56^{\circ}$ ,  $69^{\circ}$ , and  $76^{\circ}$ , corresponding to (111), (220), (311), (400), and (331) of Si, respectively [27]. Additionally, the peak at  $32^{\circ}$  is assigned to  $\text{SiO}_2$  caused by surface oxidation. The D and G peaks are characteristic Raman peaks at  $1300\text{ cm}^{-1}$  and  $1580\text{ cm}^{-1}$ ; among them,

the D peak represents the defect degree of carbon itself, and the G peak represents the degree of graphitization and the stretching vibration of the carbon material. The larger  $I_D/I_G$  value shows the lower degree of graphitization [28–32]. As displayed in Figure 2b and Figure S4b, the  $I_D/I_G$  values of Si@C<sub>Ppy</sub>-1, Si@C<sub>Ppy</sub>-2, and Si@C<sub>Ppy</sub>-3 composite are 1.03, 0.97, and 1.06, respectively, showing that the Si@C<sub>Ppy</sub>-2 material has a higher degree of graphitization and the existence of amorphous carbon [33], which can provide more reactive sites for Li<sup>+</sup> and enhance electronic conduction, and thus improve the ability to store Li<sup>+</sup>. To estimate the carbon content in the composites, thermogravimetric analysis (TGA, Figure 2c) was performed in air. The weight of the composites starts to decrease at 300 °C and decreases by 42 wt.% at 600 °C, corresponding to the carbon content of Si@C<sub>Ppy</sub>-2. A large amount of Ppy carbon material is successfully coated on the surface of silicon waste by simple chemical oxidative polymerization. To optimize the carbon content, Si@C<sub>Ppy</sub>-1 and Si@C<sub>Ppy</sub>-3 composites were synthesized. In comparison to the Si@C<sub>Ppy</sub>-2 composite, Si@C<sub>Ppy</sub>-1 and Si@C<sub>Ppy</sub>-3 composites exhibit similar morphologies (Figure S2a,c), but have different carbon weight ratios (10.12 wt.% for Si@C<sub>Ppy</sub>-1 and 32.2 wt.% for Si@C<sub>Ppy</sub>-3, Figure S5). After carbon coating of PS-Si, the type of N<sub>2</sub> adsorption/desorption curve for Si@C<sub>Ppy</sub>-2 is type IV, indicating that there are a large number of mesoporous structures (Figure 2d and Table S1). Mesopores can alleviate the volume change of Si by strain relaxation to ensure the structural integrity, thus improving the cycle stability [34].

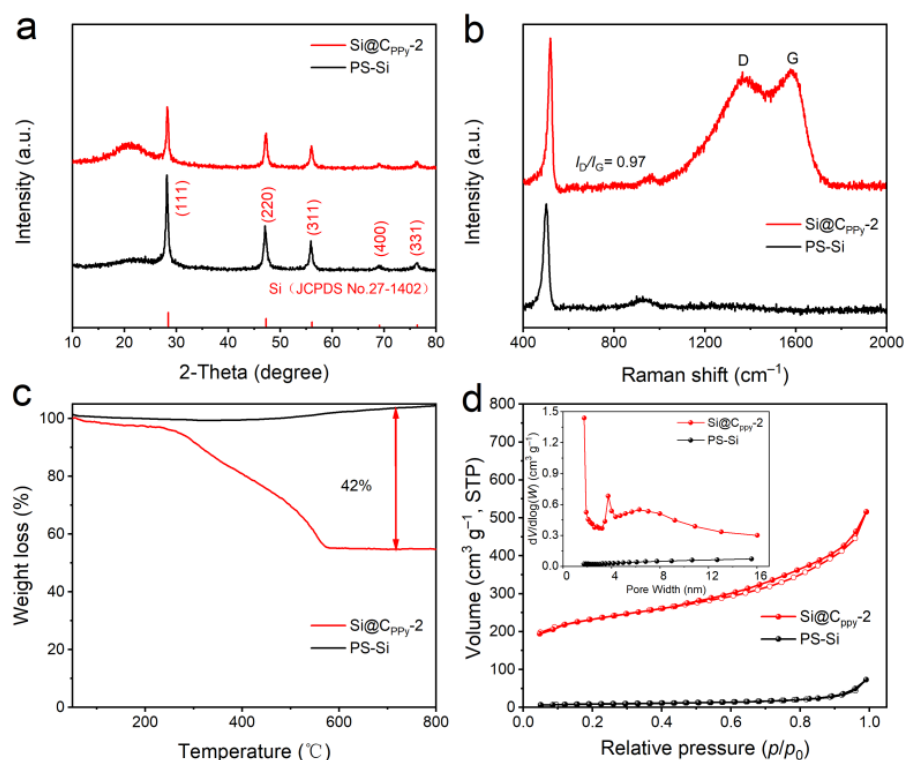


**Figure 2.** (a) XRD patterns, (b) Raman spectra, (c) TGA curves, and (d) N<sub>2</sub> adsorption–desorption isotherms with the pore size distribution of PS-Si and Si@C<sub>Ppy</sub>-2.

To verify the electrochemical performance of composites, lithium-ion half-cells were assembled with Si@C<sub>Ppy</sub>-1, Si@C<sub>Ppy</sub>-2, and Si@C<sub>Ppy</sub>-3 anode materials, respectively. The charge–discharge tests of Si@C<sub>Ppy</sub> and PS-Si anode materials were carried out at the same current density. As shown in Figure 3a, the Si@C<sub>Ppy</sub>-2 composite can maintain a high specific capacity of 335 mAh g<sup>−1</sup> and a coulombic efficiency of 99% after 200 cycles. Furthermore, the Si@C<sub>Ppy</sub>-2 composite has a high specific capacity of 1436 mAh g<sup>−1</sup> at 0.1 A g<sup>−1</sup>, and a high capacity of 607 mAh g<sup>−1</sup> even at 1.0 A g<sup>−1</sup>. At a higher current density, the discharge capacity of Si@C<sub>Ppy</sub> is higher than that of PS-Si, indicating a better rate per-

formance of Si@C<sub>ppy</sub>. In addition, when the current density is restored to 0.1 A g<sup>-1</sup>, the specific capacity of Si@C<sub>ppy</sub>-2 can still reach 778 mA h g<sup>-1</sup>, showing its excellent structural stability. Compared with silicon anode materials, the carbon-coated silicon composites achieve higher reversible capacity and CE values, which can be attributed to the improved mechanical stress and the stability of SEI layers.

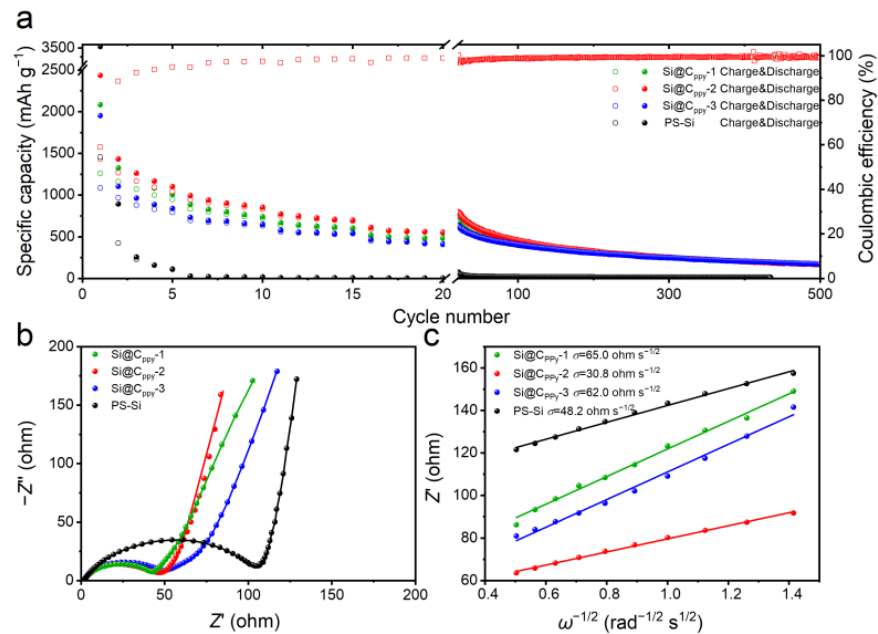


**Figure 3.** Electrochemical performance of Si@C<sub>ppy</sub> electrodes in lithium-ion half-cells. (a) Rate and cycling performance. (b) Nyquist plots. (c) Fitting  $Z'$  and  $\omega^{-1/2}$ .

To further study the electrical resistance and lithium diffusion kinetics of Si@C<sub>ppy</sub>-2 composites, EIS tests were performed. The equivalent circuit and Nyquist plots are shown in Figure 3b. The Nyquist diagrams include a semicircle and an oblique line in the high-frequency and low-frequency regions, respectively, which correspond to the charge transfer resistance ( $R_{ct}$ ) and the Warburg impedance, respectively [35,36]. As shown in Table S2, the  $R_{ct}$  value of Si@C<sub>ppy</sub>-2 (38.85 ohm) is relatively low, indicating the strong charge transfer ability of Si@C<sub>ppy</sub>-2. In addition, by fitting  $Z'$  to  $\omega^{-1/2}$  in a low-frequency  $Z_w$  region (Figure 3c), the Warburg factor ( $\sigma$ ) for PS-Si, Si@C<sub>ppy</sub>-1, Si@C<sub>ppy</sub>-2, and Si@C<sub>ppy</sub>-3 is 48.2 ohm s<sup>-1/2</sup>, 65.0 ohm s<sup>-1/2</sup>, 30.8 ohm s<sup>-1/2</sup>, and 62.0 ohm s<sup>-1/2</sup>, respectively. The ion diffusion coefficient is further calculated by  $\sigma$ , and its calculation formula is as follows:

$$D_{Li^+} = \frac{R^2 T^2}{2A^2 n^4 F^4 C^2 \sigma^2} \quad (1)$$

where  $\sigma$ ,  $\omega$ ,  $R$ ,  $T$ ,  $A$ ,  $n$ ,  $F$ , and  $C$  stand for the Warburg factor, angular frequency, gas constant, absolute temperature, electrode surface area, transfer electron number per molecule, Faraday constant, and Li<sup>+</sup> molar concentration, respectively. The  $D_{Li^+}$  of Si@C<sub>ppy</sub>-2 electrode material is about 39.56 times that of Si@C<sub>ppy</sub>-1 and 4.45 times that of Si@C<sub>ppy</sub>-3, respectively, showing that the Li<sup>+</sup> diffusion time of the Si@C<sub>ppy</sub>-2 electrode is shorter than that of the Si@C<sub>ppy</sub>-1 and Si@C<sub>ppy</sub>-3 composites. The electron transfer speed and ion diffusion kinetics of Si@C<sub>ppy</sub>-2 are faster than other electrodes, which indicates that the addition of a suitable amount of carbon can improve the rate performance of Si-based electrodes.

The electrochemical performance of Si@C<sub>ppy</sub>-2 was explored using cyclic voltammetry (CV) curves. Figure 4a shows the first three CV curves of Si@C<sub>ppy</sub>-2 composites with a scan rate of 0.1 mV s<sup>-1</sup> and a voltage window of 0.01–1.5 V. There is a wide reduction peak at 0.2V in the first cathodic scan due to the formation of SEI layer [31]. Moreover, there may be some side reactions between the electrolyte and electrode materials, leading to the increase

in irreversible charging capacity in the first cycle. In the subsequent cycles, the reduction peak at 0.2 V represents the alloying process of crystalline silicon to lithium silicon, while the two oxidation alloying peaks near 0.3 V and 0.5 V represent the de-alloying process of the  $\text{Li}_x\text{Si}$  phase as follows [34–36]:

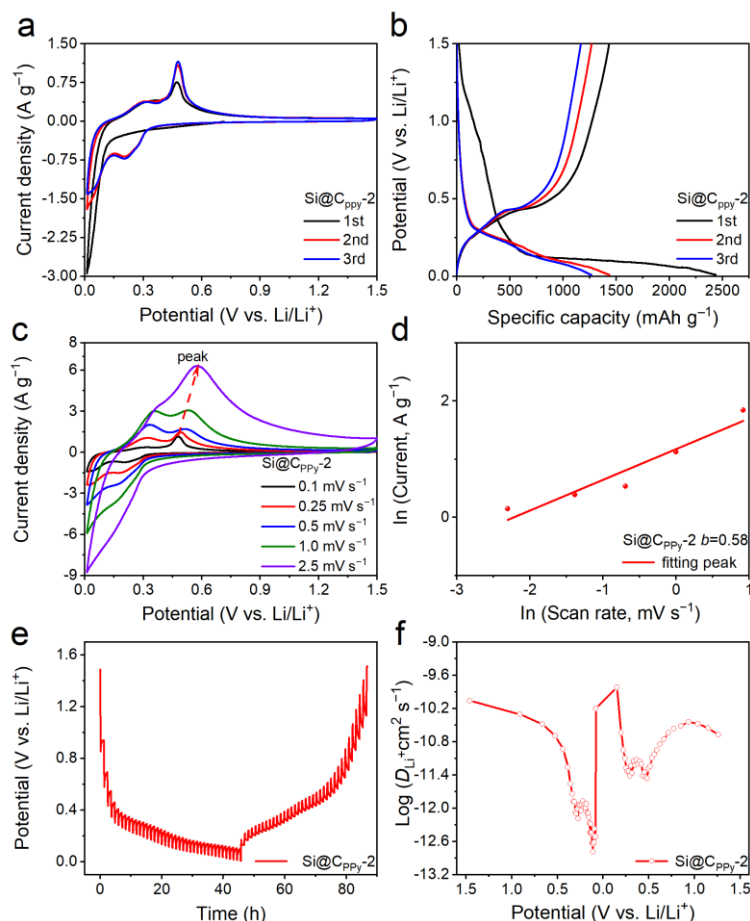


**Figure 4.** Electrochemical performance of  $\text{Si@C}_{\text{ppy-2}}$  electrode in lithium-ion half-cells. (a) CV curves at a scan rate of  $0.1 \text{ mV s}^{-1}$ . (b) The initial three GCD curves at a current density of  $0.1 \text{ A g}^{-1}$ . (c) CV curves at various scan rates from 0.1 to  $2.5 \text{ mV s}^{-1}$ . (d)  $b$ -value determination. (e) GITT curve. (f) Lithium-ion diffusion coefficient.

Figure 4b and Figure S6 exhibit the galvanostatic discharge–charge (GCD) profiles of  $\text{Si@C}_{\text{ppy}}$  composites for the initial three cycles measured at a current density of  $0.1 \text{ A g}^{-1}$  between 0.01 and 1.50 V (vs.  $\text{Li/Li}^+$ ). The first discharge specific capacity is 2083, 2433, and  $1950 \text{ mAh g}^{-1}$  for  $\text{Si@C}_{\text{ppy-1}}$ ,  $\text{Si@C}_{\text{ppy-2}}$ , and  $\text{Si@C}_{\text{ppy-3}}$ , respectively. Meanwhile, the first charge capacities of 1259, 1431, and  $1083 \text{ mAh g}^{-1}$  were obtained for  $\text{Si@C}_{\text{ppy-1}}$ ,  $\text{Si@C}_{\text{ppy-2}}$ , and  $\text{Si@C}_{\text{ppy-3}}$ , respectively.  $\text{Si@C}_{\text{ppy-1}}$ ,  $\text{Si@C}_{\text{ppy-2}}$ , and  $\text{Si@C}_{\text{ppy-3}}$  composites achieve an ICE of 60.4%, 58.8%, and 55.5%, respectively. It is known that the theoretical capacity of amorphous carbon is around  $600 \text{ mAh g}^{-1}$ , suggesting that the addition of a moderate amount of slightly graphitized carbon could suppress the fracture of silicon by increasing the electronic conductivity and deactivation of silicon anode materials. Hence, the  $\text{Si@C}_{\text{ppy-2}}$  composite delivers a higher specific capacity.

To deeply study the storage kinetics of lithium ions, the CV curves of the three composites at different scan rates were recorded. As shown in Figures 4c and S7, the CV curves of the three samples were similar, with one reduction peak and two oxidation peaks (from 0.1 to  $2.5 \text{ mV s}^{-1}$ ). The peak current ( $i$ ) and the scan rate ( $v$ ) have a relationship

according to Equation (3), where  $i$  is the peak current,  $v$  is the scan rate,  $a$  and  $b$  are constants. The  $b$  value can be calculated from the slope of  $\log(i)$ – $\log(v)$  and reflect the electrochemical reaction kinetics of Li-ion batteries.

$$i = av^b \quad (3)$$

$$\log(i) = b\log(v) + \log(a) \quad (4)$$

It is worth pointing out that  $b = 0.5$  indicates diffusion-controlled reactions, while  $b = 1$  means surface-controlled reactions. As shown in Figure 4d, the  $b$  value of the Si@C<sub>PPy</sub>-2 composite is 0.58, which is closer to 0.5, suggesting that the diffusion-dominating process controls the lithium storage dynamics.

The galvanostatic intermittent titration technique (GITT) was applied to investigate the diffusion coefficient of Li-ions ( $D_{Li^+}$ ) by applying a pulse current at 0.1 A g<sup>−1</sup> for 10 min and standing for 1 h (Figure 4e). The  $D_{Li^+}$  can be calculated by the formula as follows:

$$D_{Li^+} = \frac{4}{\pi\tau} \left( \frac{m_b V_M}{M_B S} \right)^2 \left( \frac{\Delta E_S}{\Delta E_\tau} \right)^2 \quad (5)$$

where  $m_b$  and  $M_B$  represent the active mass and molar mass, respectively.  $\tau$  represents the pulse time, and  $V_M$  and  $S$  represent the molar volume of the electrode sheet and the surface area of the active mass, respectively. Additionally,  $\Delta E_S$  and  $\Delta E_\tau$  represent pulse-induced voltage changes and galvanostatic charge–discharge voltage changes, respectively [37]. As shown in Figure 4f, in the lithiation process, the  $D_{Li^+}$  of the Si@C<sub>PPy</sub>-2 composite is 10<sup>−9.5</sup>–10<sup>−13</sup> cm<sup>2</sup> s<sup>−1</sup>. These values are 100 times that of PS-Si. It can be seen that the Si@C<sub>PPy</sub>-2 composite has faster diffusion kinetics [38,39]. In short, the good electrochemical performance of the Si@C<sub>PPy</sub>-2 composite is attributed to its unique structural features: (i) porous structure and protective carbon layer can help to slow down the volume changes of silicon during lithiation/delithiation, and (ii) the large specific surface area (SSA) can provide sufficient electrode/electrolyte contact area, while the porous structure facilitates electrolyte penetration and ion transport, thereby accelerating Li<sup>+</sup> diffusion transfer during the discharge-charge process. Therefore, carbon coating is beneficial for improving the electrochemical performance of PS-Si and ensuring the integrity of the overall structure of the anode electrode material, thereby achieving an excellent lithium storage capacity.

#### 4. Conclusions

In summary, Si@C<sub>PPy</sub> composites are successfully fabricated by annealing PPy. The carbon layer can alleviate the pulverization and expansion problem of Si during the lithiation/delithiation process, leading to a stable electrochemical performance. In addition, the carbon coating can increase the electrode/electrolyte contact area by increasing the SSA of the anode material. Moreover, the Si@C<sub>PPy</sub> composites possess mesoporous structures and excellent electrical conductivity, which can deliver an excellent cycling performance. The Si@C<sub>PPy</sub>-2 composite can still exhibit a high specific capacity of 460 mAh g<sup>−1</sup> after 100 cycles, while the specific capacity of PS-Si is only 18 mAh g<sup>−1</sup>. Hence, this work not only provides an effective way for the high-value utilization of PV Si waste, but also opens a new strategy for designing alloying-type anode materials for energy storage.

**Supplementary Materials:** The following supporting information can be downloaded at: <https://www.mdpi.com/article/10.3390/nano13142142/s1>. Figure S1: Illustration of the preparation process of Si@C<sub>PPy</sub> materials; Figure S2: SEM of (a) Si@C<sub>PPy</sub>-1, (b) Si@C<sub>PPy</sub>-2, and (c) Si@C<sub>PPy</sub>-3; Figure S3: SEM images of (a) Raw-Si and (b) PS-Si; Figure S4: (a) XRD patterns and (b) Raman spectra of Si@C<sub>PPy</sub>-1 and Si@C<sub>PPy</sub>-3; Figure S5: TGA curves of PS-Si, Si@C<sub>PPy</sub>-1, and Si@C<sub>PPy</sub>-3; Figure S6: (a,b) Discharge–charge profiles of Si@C<sub>PPy</sub>-1 and Si@C<sub>PPy</sub>-3 at 0.1 A g<sup>−1</sup>; Figure S7: (a,b) CV curves of Si@C<sub>PPy</sub>-1 and Si@C<sub>PPy</sub>-3 at various scan rates; Table S1: BET specific surface area, pore volume, and BJH pore size of PS-Si and Si@C<sub>PPy</sub>-2; and Table S2:  $R_s$  and  $R_{ct}$  values of Si@C<sub>PPy</sub>-1, Si@C<sub>PPy</sub>-2, and Si@C<sub>PPy</sub>-3.

**Author Contributions:** Conceptualization, J.H. and J.L. (Jun Li); methodology, J.H. and J.L. (Jun Li); validation, J.H., J.L. (Jun Li) and L.Y.; formal analysis, J.H. and Y.C.; investigation, J.H. and J.L. (Jun Li); data curation, J.H. and M.W.; writing—original draft preparation, J.H.; writing—review and editing, H.L., J.L. (Jiabiao Lian) and C.W.; visualization, J.H.; supervision, J.L. (Jiabiao Lian) and C.W.; funding acquisition, Y.C., J.L. (Jiabiao Lian) and C.W. All authors have read and agreed to the published version of the manuscript.

**Funding:** This work was supported by the Nanjing Tech University Research Start-up Fund (3824017111), the China Postdoctoral Science Foundation (2022M711381), and the National Natural Science Foundation of China (21706103).

**Institutional Review Board Statement:** Not applicable.

**Informed Consent Statement:** Not applicable.

**Data Availability Statement:** Not applicable.

**Conflicts of Interest:** The authors declare no conflict of interest.

## References

1. Yoshikawa, K.; Kawasaki, H.; Yoshida, W.; Irie, T.; Konishi, K.; Nakano, K.; Uto, T.; Adachi, D.; Kanematsu, M.; Uzu, H.; et al. Silicon heterojunction solar cell with interdigitated back contacts for a photoconversion efficiency over 26%. *Nat. Energy* **2017**, *2*, 17032. [[CrossRef](#)]
2. Zhang, X.; Wang, D.; Qiu, X.; Ma, Y.; Kong, D.; Müllen, K.; Li, X.; Zhi, L. Stable high-capacity and high-rate silicon-based lithium battery anodes upon two-dimensional covalent encapsulation. *Nat. Commun.* **2020**, *11*, 3826. [[CrossRef](#)]
3. Shang, H.; Zuo, Z.; Yu, L.; Wang, F.; He, F.; Li, Y. Low-temperature growth of all-carbon graphdiyne on a silicon anode for high-performance lithium-ion batteries. *Adv. Mater.* **2018**, *30*, 1801459. [[CrossRef](#)] [[PubMed](#)]
4. Zuo, X.; Zhu, J.; Müller-Buschbaum, P.; Cheng, Y.J. Silicon based lithium-ion battery anodes: A chronicle perspective review. *Nano Energy* **2017**, *31*, 113–143. [[CrossRef](#)]
5. Hu, J.Z.; Liu, W.J.; Zheng, J.H.; Li, G.C.; Bu, Y.F.; Qiao, F.; Lian, J.B.; Zhao, Y. Coral-like cobalt selenide/carbon nanosheet arrays attached on carbon nanofibers for high-rate sodium-ion storage. *Rare Met.* **2023**, *42*, 916–928. [[CrossRef](#)]
6. Park, S.J.; Zhao, H.; Ai, G.; Wang, C.; Song, X.; Yuca, N.; Battaglia, V.S.; Yang, W.; Liu, G. Side-chain conducting and phase-separated polymeric binders for high-performance silicon anodes in lithium-ion batteries. *J. Am. Chem. Soc.* **2015**, *137*, 2565–2571. [[CrossRef](#)]
7. He, Y.; Xu, G.; Wang, C.; Xu, L.; Zhang, K. Horsetail-derived Si@N-doped carbon as low-cost and long cycle life anode for Li-ion half/full cells. *Electrochim. Acta* **2018**, *264*, 173–182. [[CrossRef](#)]
8. Kang, R.; Zhu, W.Q.; Li, S.; Zou, B.B.; Li, G.C.; Liu, X.H.; Ng, D.H.L.; Qiu, J.X.; Zhao, Y.; Qiao, F.; et al. Fe<sub>2</sub>TiO<sub>5</sub> nanochains as anode for high-performance lithium-ion capacitor. *Rare Met.* **2021**, *40*, 2424–2431. [[CrossRef](#)]
9. Ma, Y.; Guo, P.; Liu, M.; Cheng, P.; Zhang, T.; Liu, J.; Liu, D.; He, D. To achieve controlled specific capacities of silicon-based anodes for high-performance lithium-ion batteries. *J. Alloys Compd.* **2022**, *905*, 164189. [[CrossRef](#)]
10. Xie, Y.; He, C.; Zhang, J.; Hou, Y.; Meng, W.; Zhao, D. Nitrogen-doped carbon caging silicon nanoparticles for high performance lithium-ion battery anodes. *J. Alloys Compd.* **2021**, *860*, 158487. [[CrossRef](#)]
11. El-Khodary, S.A.; Subburam, G.; Zou, B.B.; Wang, J.; Qiu, J.X.; Liu, X.H.; Ng, D.H.L.; Wang, S.; Lian, J.B. Mesoporous silica anchored on reduced graphene oxide nanocomposite as anode for superior lithium-ion capacitor. *Rare Met.* **2022**, *41*, 368–377. [[CrossRef](#)]
12. Shi, F.; Song, Z.; Ross, P.N.; Somorjai, G.A.; Ritchie, R.O.; Komvopoulos, K. Failure mechanisms of single-crystal silicon electrodes in lithium-ion batteries. *Nat. Commun.* **2016**, *7*, 11886. [[CrossRef](#)] [[PubMed](#)]
13. Yao, M.; Zeng, Z.; Zhang, H.; Yan, J.; Liu, X. Electrophoretic deposition of carbon nanofibers/silicon film with honeycomb structure as integrated anode electrode for lithium-ion batteries. *Electrochim. Acta* **2018**, *281*, 312–322. [[CrossRef](#)]
14. Sun, W.; Hu, R.; Zhang, M.; Liu, J.; Zhu, M. Binding of carbon coated nano-silicon in graphene sheets by wet ball-milling and pyrolysis as high performance anodes for lithium-ion batteries. *J. Power Sources* **2016**, *318*, 113–120. [[CrossRef](#)]
15. Jiang, T.; Zhang, R.; Yin, Q.; Zhou, W.; Dong, Z.; Chernova, N.A.; Wang, Q.; Omenya, F.; Whittingham, M.S. Morphology, composition and electrochemistry of a nano-porous silicon versus bulk silicon anode for lithium-ion batteries. *J. Mater. Sci.* **2017**, *54*, 3670–3677. [[CrossRef](#)]
16. Zhang, Y.; Li, K.; Ji, P.; Chen, D.; Zeng, J.; Sun, Y.; Zhang, P.; Zhao, J. Silicon-multi-walled carbon nanotubes-carbon microspherical composite as high-performance anode for lithium-ion batteries. *J. Mater. Sci.* **2017**, *52*, 3630–3641. [[CrossRef](#)]
17. Li, S.; Wang, T.; Zhu, W.; Lian, J.; Huang, Y.; Yu, Y.; Qiu, J.; Zhao, Y.; Yong, Y.; Li, H. Controllable synthesis of uniform mesoporous H-Nb<sub>2</sub>O<sub>5</sub>/rGO nanocomposites for advanced lithium-ion hybrid supercapacitors. *J. Mater. Chem. A* **2019**, *7*, 693–703. [[CrossRef](#)]
18. Li, S.; Wang, T.; Huang, Y.; Wei, Z.; Li, G.; Ng, D.H.L.; Lian, J.; Qiu, J.; Zhao, Y.; Zhang, X.; et al. Porous Nb<sub>4</sub>N<sub>5</sub>/rGO nanocomposite for ultrahigh-energy-density lithium-ion hybrid capacitor. *ACS Appl. Mater. Interfaces* **2019**, *11*, 24114–24121. [[CrossRef](#)]

19. Chen, S.; Shen, L.; Peter, A.; Maier, J.; Yu, Y. Dual-functionalized double carbon shells coated silicon nanoparticles for high performance lithium-ion batteries. *Adv. Mater.* **2017**, *29*, 1605650. [[CrossRef](#)]
20. Zou, B.; Li, S.; Wang, J.; Li, G.; Zhao, Y.; Qiu, J.; Ng, D.H.L.; Liu, X.; Lian, J.; Li, H. A general strategy towards transition metal nitrides (TMNs)/rGO nanocomposites for superior lithium ion storage. *J. Alloys Compd.* **2021**, *865*, 158968. [[CrossRef](#)]
21. Qi, C.; Li, S.; Yang, Z.; Xiao, Z.; Zhao, L.; Yang, F.; Ning, G.; Ma, X.; Wang, C.; Xu, J.; et al. Suitable thickness of carbon coating layers for silicon anode. *Carbon* **2022**, *186*, 530–538. [[CrossRef](#)]
22. Gao, L.; Huang, T.; Cui, M.; Xu, J.; Xiao, R. Facile and efficient fabrication of branched Si@C anode with superior electrochemical performance in LIBs. *Small* **2021**, *17*, 2005997.
23. Huang, X.; Ding, Y.; Li, K.; Guo, X.; Zhu, Y.; Zhang, Y.; Bao, Z. Spontaneous formation of the conformal carbon nanolayer coated Si nanostructures as the stable anode for lithium-ion batteries from silica nanomaterials. *J. Power Sources* **2021**, *496*, 229833. [[CrossRef](#)]
24. Li, D.; Zhang, M.; Zhang, L.; Xu, X.; Pan, Q.; Huang, Y.; Zheng, F.; Wang, H.; Li, Q. Constructing three-dimensional N-doped carbon coating silicon/iron silicide nanoparticles cross-linked by carbon nanotubes as advanced anode materials for lithium-ion batteries. *J. Colloid Interface Sci.* **2023**, *629*, 908–916. [[CrossRef](#)] [[PubMed](#)]
25. Jung, C.; Choi, J.; Kim, W.S.; Hong, S.H. A nanopore-embedded graphitic carbon shell on silicon anode for high performance lithium ion batteries. *J. Mater. Chem. A* **2018**, *6*, 8013–8020. [[CrossRef](#)]
26. Yi, Y.; Lee, G.H.; Kim, J.C.; Shim, H.W.; Kim, D.W. Tailored silicon hollow spheres with Micrococcus for Li ion battery electrodes. *Chem. Eng. J.* **2017**, *327*, 297–306. [[CrossRef](#)]
27. Chen, Y.; Hu, Y.; Shen, Z.; Chen, R.; He, X.; Zhang, X.; Zhang, Y.; Wu, K. Sandwich structure of graphene-protected silicon/carbon nanofibers for lithium-ion battery anodes. *Electrochim. Acta* **2016**, *210*, 53–60. [[CrossRef](#)]
28. Wang, J.; El-Khodary, S.A.; Ng, D.H.L.; Li, S.; Cui, Y.X.; Zou, B.B.; Liu, X.H.; Lian, J.B. Kinetic analysis of bio-oil derived hierarchically porous carbon for superior Li<sup>+</sup>/Na<sup>+</sup> storage. *J. Phys. Chem. Lett.* **2022**, *13*, 7273–7279. [[CrossRef](#)] [[PubMed](#)]
29. Wang, L.L.; Wang, J.; Ng, D.H.L.; Li, S.; Zou, B.B.; Cui, Y.X.; Liu, X.H.; El-Khodary, S.A.; Qiu, J.X.; Lian, J.B. Operando mechanistic and dynamic studies of N/P co-doped hard carbon nanofibers for efficient sodium storage. *Chem. Commun.* **2021**, *57*, 9610–9613. [[CrossRef](#)]
30. Zhu, W.Q.; El-Khodary, S.A.; Li, S.Y.; Zou, B.B.; Kang, R.; Li, G.C. Roselle-like Zn<sub>2</sub>Ti<sub>3</sub>O<sub>8</sub>/rGO nanocomposite as anode for lithium ion capacitor. *Chem. Eng. J.* **2020**, *385*, 123881. [[CrossRef](#)]
31. An, Y.; Fei, H.; Zeng, G.; Ci, L.; Xiong, S.; Feng, J.; Qian, Y. Green, scalable, and controllable fabrication of nanoporous silicon from commercial alloy precursors for high-energy lithium-ion batteries. *ACS Nano* **2018**, *12*, 4993–5002. [[CrossRef](#)] [[PubMed](#)]
32. Feng, J.; Zhang, Z.; Ci, L.; Zhai, W.; Ai, Q.; Xiong, S. Chemical dealloying synthesis of porous silicon anchored by in situ generated graphene sheets as anode material for lithium-ion batteries. *J. Power Sources* **2015**, *287*, 177–183. [[CrossRef](#)]
33. Pang, C.; Cui, H.; Yang, G.; Wang, C. Flexible transparent and free-standing silicon nanowires paper. *Nano Lett.* **2013**, *13*, 4708–4714. [[CrossRef](#)] [[PubMed](#)]
34. Liu, N.; Lu, Z.; Zhao, J.; McDowell, M.T.; Lee, H.W.; Zhao, W.; Cui, Y. A pomegranate-inspired nanoscale design for large-volume-change lithium battery anodes. *Nat. Nanotechnol.* **2014**, *9*, 187–192. [[CrossRef](#)] [[PubMed](#)]
35. Yin, S.; Zhao, D.; Ji, Q.; Xia, Y.; Xia, S.; Wang, X.; Wang, M.; Ban, J. Si/Ag/C Nanohybrids with in situ incorporation of super-small silver nanoparticles: Tiny amount, huge impact. *ACS Nano* **2018**, *12*, 861–875. [[CrossRef](#)]
36. Kovalenko, I.; Zdyrko, B.; Magasinski, A.; Hertzberg, B.; Milicevic, Z.; Burtovyy, R.; Luzinov, I.; Yushin, G. A major constituent of brown algae for use in high-capacity Li-ion batteries. *Science* **2011**, *334*, 75–79. [[CrossRef](#)]
37. Zou, B.B.; Zhang, W.; Cui, Y.X.; Li, S.; Li, G.C.; Liu, X.H.; Ng, D.H.L.; Qiu, J.X.; Lian, J.B. Interfacial engineering for metal oxides/nitrides nano-heterojunctions towards high-rate lithium-ion storage. *J. Mater. Chem. A* **2022**, *10*, 7391–7398. [[CrossRef](#)]
38. Kwon, H.J.; Hwang, J.Y.; Shin, H.J.; Jeong, M.G.; Chung, K.Y.; Sun, Y.K.; Jung, H.G. Nano/microstructured silicon-carbon hybrid composite particles fabricated with corn starch biowaste as anode materials for Li-ion batteries. *Nano Lett.* **2020**, *20*, 625–635. [[CrossRef](#)]
39. Ji, H.S.; Li, J.; Li, S.; Cui, Y.X.; Liu, Z.J.; Huang, M.G.; Xu, C.; Li, G.C.; Zhao, Y.; Li, H.M. High-value utilization of silicon cutting waste and excrementum bombycis to synthesize silicon-carbon composites as anode materials for Li-ion batteries. *Nanomaterials* **2022**, *12*, 2875. [[CrossRef](#)]

**Disclaimer/Publisher's Note:** The statements, opinions and data contained in all publications are solely those of the individual author(s) and contributor(s) and not of MDPI and/or the editor(s). MDPI and/or the editor(s) disclaim responsibility for any injury to people or property resulting from any ideas, methods, instructions or products referred to in the content.